Journal of *Marine Science and Engineering*

MDPI

Article

Research on Time–Frequency Joint Equalization Algorithm for Underwater Acoustic FBMC/OQAM Systems

Weimin Hou [1], Ming Zhang [1], Lin Yang [1] and Yanxia Wang [2,*]

[1] School of Information Science and Engineering, Hebei University of Science and Technology, Shijiazhuang 050018, China; hwm@hebust.edu.cn (W.H.); zhangming5280@126.com (M.Z.); yanglincl626@163.com (L.Y.)
[2] School of Electrical Engineering, Hebei University of Architecture, Zhangjiakou 075132, China
* Correspondence: yanxiawang2023@163.com

Abstract

This study focuses on the equalization problem of the filter bank multicarrier system based on offset quadrature amplitude modulation (FBMC/OQAM) in underwater acoustics and proposes an innovative joint time–frequency-domain equalization (JTFDE) algorithm. The algorithm combines frequency-domain Minimum Mean Square Error (MMSE) equalization with time-domain adaptive decision feedback equalization, effectively addressing the shortcomings of traditional single-domain equalization methods in terms of multipath interference suppression and time-varying channel tracking. By first using frequency-domain linear equalization to preliminarily eliminate multipath interference, and then combining it with time-domain Recursive Least Squares (RLS) adaptive decision feedback to further suppress residual interference, the system performance is significantly improved. The experimental results show that compared with existing single-domain equalization methods, this scheme reduces the bit error rate at the system receiver and enhances the system's interference resistance.

Keywords: FBMC/OQAM; frequency-domain equalization; time-domain equalization; joint time-frequency equalization; underwater acoustic communication

check for updates

Academic Editor: Guoqing Zhang

Received: 12 August 2025
Revised: 9 September 2025
Accepted: 13 September 2025
Published: 15 September 2025

Citation: Hou, W.; Zhang, M.; Yang, L.; Wang, Y. Research on Time–Frequency Joint Equalization Algorithm for Underwater Acoustic FBMC/OQAM Systems. *J. Mar. Sci. Eng.* **2025**, *13*, 1781. https://doi.org/10.3390/jmse13091781

Copyright: © 2025 by the authors. Licensee MDPI, Basel, Switzerland. This article is an open access article distributed under the terms and conditions of the Creative Commons Attribution (CC BY) license (https://creativecommons.org/licenses/by/4.0/).

1. Introduction

In recent years, with the rapid development of the Internet of Underwater Things (IoUT) and marine communication technologies, the demand for transmission quality and rate in underwater acoustic communication has been continuously increasing [1]. Multi-carrier modulation technology has become a research hotspot in high-speed underwater communication due to its characteristics of anti-multipath interference and high spectral efficiency [2]. Among them, the filter bank multicarrier (FBMC) technology based on offset quadrature amplitude modulation (OQAM) is regarded as a potential alternative to the traditional orthogonal frequency division multiplexing (OFDM) technology, owing to its excellent anti-interference capability, low out-of-band leakage, and high spectral efficiency [3].

However, the filter bank multicarrier system based on offset quadrature amplitude modulation (FBMC/OQAM) faces two core challenges in practical applications [4]: first, the time-varying and sparse characteristics of the underwater acoustic channel significantly increase the difficulty of channel estimation and equalization [5,6]; second, the system's inherent imaginary interference problem makes traditional OFDM equalization algorithms

inapplicable directly [7,8]. Specifically, the underwater acoustic channel has complex multipath effects and Doppler frequency shifts, leading to severe inter-symbol interference (ISI) and inter-carrier interference (ICI) during signal transmission [9]. In addition, the FBMC/OQAM system can only ensure orthogonality in the real domain, and the existence of imaginary interference further increases the complexity of signal processing at the receiving end [10].

Regarding the aforementioned issues, existing research primarily focuses on single-domain equalization methods [5,8,11], such as Zero-Forcing (ZF) equalization [12], Minimum Mean Square Error (MMSE) equalization [13], Recursive Least Squares (RLS) equalization [14], and Least Mean Square (LMS) equalization [15]. Although frequency-domain equalization offers high computational efficiency, it has insufficient capability to track time-varying channels [16]; in contrast, time-domain adaptive equalization can dynamically adjust parameters, yet its effectiveness in suppressing multipath interference is limited [17]. In recent years, time–frequency joint equalization algorithms have attracted widespread attention due to their ability to synergistically leverage the rapidity of frequency-domain processing and the robustness of time-domain equalization, demonstrating significant potential to enhance system performance. For instance, Ruigang et al. [17] proposed a Time-Domain Adaptive Decision Feedback Equalization (TD-ADFE) for Shift Keying (MSK) signals in time-varying underwater acoustic channels. This method is based on Laurent decomposition and updates the equalizer coefficients iteratively to track channel variations, achieving improved bit error performance compared to Frequency-Domain Block Linear Equalization (FD-BLE). Han et al. [18] further developed time–frequency joint equalization (JTFDE), which combines FD-BLE with TD-ADFE. It exhibits excellent performance in suppressing ISI and tracking time-varying channel characteristics, significantly improving the system bit error rate. In addition, Kadhem et al. [16] investigated a range of equalization schemes suitable for FBMC/OQAM systems and assessed their bit error performance under typical channel conditions. However, most of these studies focus on single-domain equalization algorithms tailored to MSK or FBMC/OQAM systems, and do not fully address the inherent imaginary interference and real-domain orthogonality constraints of underwater acoustic FBMC/OQAM systems. Consequently, residual interference and performance degradation persist in channels characterized by high sparsity and strong multipath effects.

To address the aforementioned challenges, this paper proposes a novel time–frequency joint equalization (JTFDE) scheme tailored for underwater acoustic scenarios. While the concept of time–frequency joint processing has been adopted in other communication systems [18], existing studies have failed to systematically resolve the inherent imaginary interference and real-domain orthogonality constraints specific to underwater acoustic FBMC/OQAM systems. Innovatively, this scheme employs a cascaded architecture integrating frequency-domain pre-equalization and time-domain adaptive decision feedback: it first provides preliminary suppression of multipath interference via frequency-domain processing, then achieves dynamic channel tracking and residual interference cancellation through time-domain processing, and specifically mitigates the system-specific imaginary interference by incorporating iterative interference cancellation technology.

2. Underwater Acoustics FBMC/OQAM System Model

2.1. Design of Prototype Pulses

The design of the prototype pulse determines the performance of the underwater acoustic FBMC/OQAM system. The better its time–frequency localization characteristics, the more concentrated the energy is in the time–frequency domain, resulting in less energy leakage into adjacent time–frequency domains and stronger interference resistance. Therefore, selecting an appropriate prototype pulse is crucial for different underwater acoustic

channels. Some European universities and research institutions have collaborated on the Physical Layer for Dynamic Spectrum Access (PHYDYAS) project, proposing a prototype pulse based on frequency sampling technology. This study is based on the PHYDYAS prototype pulse. In addition, there are some high-performance prototype pulses, such as the Extended Gauss Filter, which can adjust pulse parameters based on channel characteristics to reduce channel interference. The common goal of these prototype pulses is to reduce out-of-band attenuation; so, it is generally necessary to increase the filter order. In this study, based on the PHYDYAS prototype pulse, an overlap factor K is introduced, where K is the ratio of the prototype pulse length to the number of subcarriers M. Assuming that the filter coefficient corresponding to the center frequency of the PHYDYAS pulse is H_0, and the filter coefficient at a distance i from the center frequency is H_i, Table 1 shows the prototype pulse coefficients corresponding to several typical values of the overlap factor.

Table 1. Prototype filter frequency-domain sampling coefficient.

Overlap Factor	**Filter Coefficients**			
K	H0	H1	H2	H3
2	1	$\sqrt{2}/2$	—	—
3	1	0.911438	0.411438	—
4	1	0.971860	$\sqrt{2}/2$	0.235147

The formula is as follows:

$$g[i] = \begin{cases} H_0 + 2\sum_{k=1}^{K-1} H_i \cos\left(2\pi \frac{k}{KM} i\right), & 1 \le i \le KM-1 \\ 0 \quad , & \text{else} \end{cases} \tag{1}$$

Figure 1 shows the time–frequency characteristics of the PHYDYAS prototype pulse for overlap factors of 2, 3, and 4. By observing the time-domain waveform and amplitude-frequency response of PHYDYAS, it was found that the larger the overlap factor, the smaller the out-of-band attenuation.

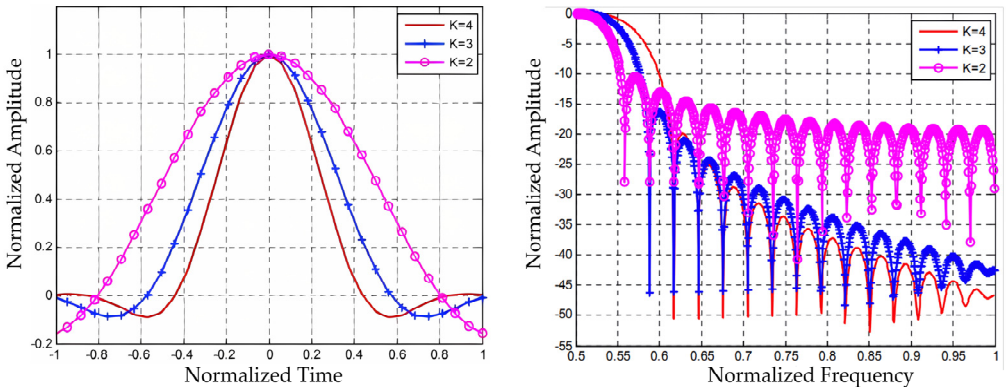


Figure 1. Time–frequency characteristics of PHYDYAS under different overlap factors K. (**a**) PHYDYAS time-domain waveforms under different overlap factors K; (**b**) PHYDYAS amplitude–frequency response under different overlap factors K.

In summary, the inherent imaginary-part interference of FBMC/OQAM systems can be minimized by optimally designing prototype filter, which also provides a theoretical basis for the system's orthogonality under ideal static channel conditions. The equalizer proposed later in this paper, on the other hand, is mainly used to suppress additional interference introduced by practical underwater acoustic channels (such as multipath, time

variation, and Doppler effect). These two components (the optimized prototype filter and the proposed equalizer) have distinct focuses in their objectives and clear hierarchical roles, and they work together to improve the overall performance of the system in harsh underwater acoustic environments.

2.2. Offset Quadrature Amplitude Modulation

The prototype pulse filter design of the FBMC system sacrifices strict orthogonality between subcarriers; so, the receiving end will inevitably be affected by the overlapping parts of adjacent subcarriers. Interference between adjacent filters is called interference filters, and the interference coefficient can be expressed by the product of the filter frequency coefficients [19], as shown in Equation (2):

$$G_k = H_k H_{K-k} \quad k = 1, 2, \ldots, K-1 \tag{2}$$

when K = 4, the interference coefficients are $G_1 = G_3 = 0.2285$ and $G_2 = 0.5$, respectively, and the frequency-domain response of the interference filter can be expressed by Equation (3):

$$G(f) = \sum_{k=1}^{K-1} G_k \frac{\sin\left(\pi\left(f - \frac{k}{MK}\right)MK\right)}{MK \sin\left(\pi\left(f - \frac{k}{MK}\right)\right)} \tag{3}$$

The time-domain response $g(t)$ of the interference filter can be obtained by performing an inverse Fourier transform on the frequency response, as expressed in Equation (4):

$$g(t) = \left[G_2 + 2G_1 \cos\left(\frac{2\pi kt}{KT}\right)\right] e^{j2\pi \frac{t}{2T}} \tag{4}$$

In Equation (4), T represents the time-domain period of the signal. The first term of the product on the right-hand side of the equation is a complex exponential, and the second term is a real number. According to Euler's formula, when t is an even multiple of $T/2$, $g(t)$ is purely imaginary; when t is an odd multiple of $T/2$, $g(t)$ is purely real. Therefore, only one form of interference exists between adjacent subcarriers. To visually demonstrate this characteristic, the real and imaginary parts of the interference filter's time-domain response curves are plotted in Figure 2. Figure 3 compares the frequency-domain response characteristics of the prototype filter and the interference filter.

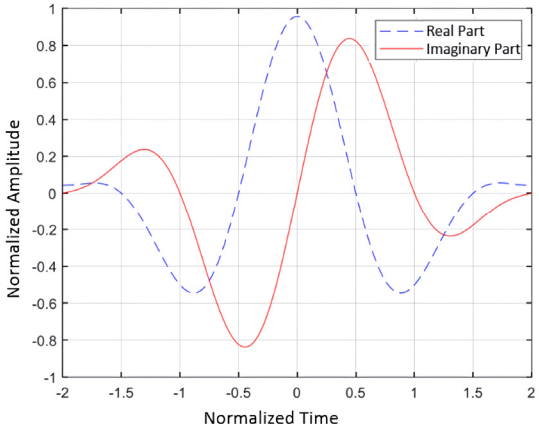


Figure 2. Time-domain response of interference filter.

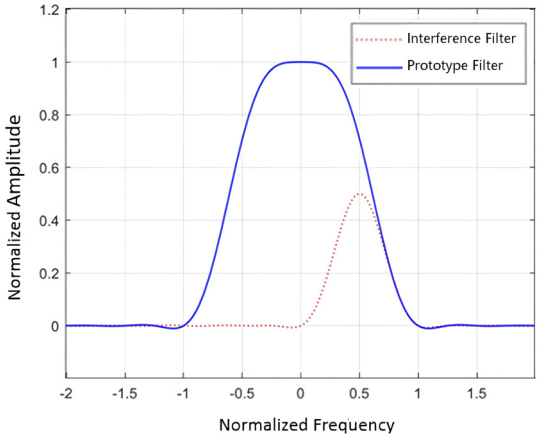


Figure 3. Frequency-domain response of prototype filters and interference filters.

Table 2 shows the time-domain interference values of the interference filter when $K = 4$. As can be seen from the table, the interference terms alternate between real and imaginary. To avoid interference between subcarriers, it is necessary to avoid the simultaneous use of adjacent subcarriers. However, this method results in a subcarrier utilization rate of only 50%, severely wasting spectrum resources. By leveraging the alternating real and imaginary nature of the interference filter, OQAM technology can be employed to avoid interference at sampling points, thereby fully utilizing spectrum resources. OQAM improves upon conventional quadrature amplitude modulation (QAM) by separating the real and imaginary components of the modulated signal, thereby preventing interference between adjacent subcarriers. The working principle of OQAM is as follows: the signal undergoes QAM modulation, then the real and imaginary components of the modulated signal are separated, and the two data streams are transmitted with a delay of T/2; at the receiving end, the use of the same delay can effectively avoid interference between subcarriers, as shown in Figure 4.

Table 2. Time-domain interference values of the filter at $K = 4$.

f \ t	−2	−3/2	−1	−1/2	0	1/2	2	3/2	2
2	0	−0.0006	−0.0001	0	0	0	−0.0001	−0.0006	0
1	−0.0054	−*j*0.0429	0.1250	*j*0.2058	−0.2393	−j0.2058	0.1250	*j*0.0429	−0.0054
0	0	0.0668	0.0002	−0.5644	1	−0.5644	0.0002	0.0668	0
1	−0.0054	*j*0.0429	0.1250	−*j*0.2058	−0.2393	*j*0.2058	0.1250	−*j*0.0429	−0.0054
2	0	−0.0006	−0.0001	0	0	0	−0.0001	−0.0006	0

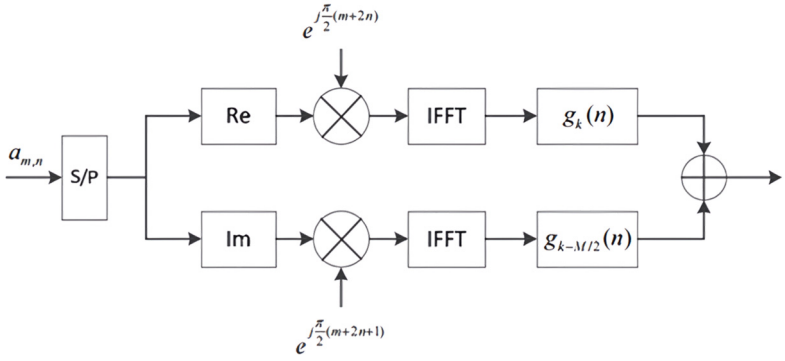


Figure 4. OQAM flowchart.

$$\langle g_{m,n}, g_{m_0,n_0} \rangle_R = \begin{cases} A_g((n_0-n)\tau_0, (m-m_0)\nu_0)(m-m_0, n_0-n)\text{mod}2 = (0,0) \\ 0 \qquad\qquad\qquad\qquad\qquad\qquad (m-m_0, n_0-n)\text{mod}2 \neq (0,0) \end{cases} \tag{5}$$

The real-domain inner product function of the transmitter and receiver ends of the FBMC communication system [20] can be expressed as in Equation (5).From this equation, it can be seen that the parity of the time–frequency grid point coordinates (m, n) can divide the grid points into four different types: even–even, odd–even, even–odd, and odd–odd. This means that both the time domain and frequency domain exhibit an alternating pattern of real and imaginary values, as shown in Figure 5. This modulation method avoids interference between adjacent subcarriers while maximizing the interference distance in the time–frequency space. OQAM is well suited to FBMC systems, minimizing self-interference in FBMC systems, effectively utilizing spectrum resources, and improving transmission efficiency.

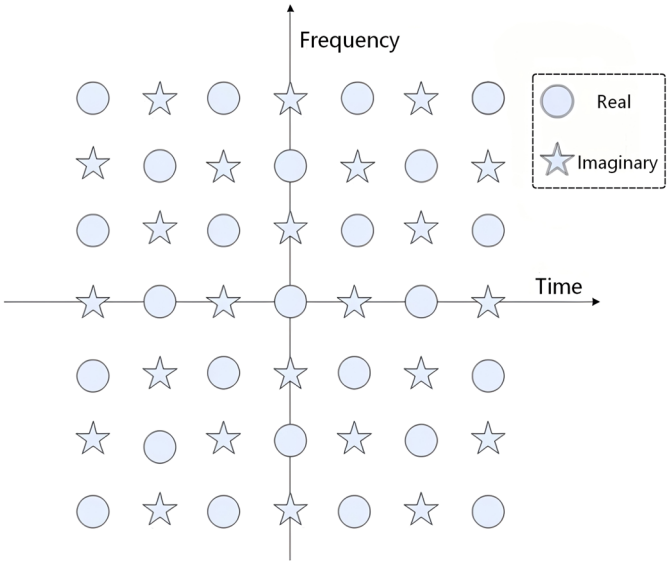


Figure 5. OQAM grid plot.

2.3. FBMC System Rapid Implementation

One of the key factors contributing to the widespread application of OFDM technology is that it can be implemented using methods based on the inverse fast Fourier transform (IFFT) and fast Fourier transform (FFT), significantly reducing computational complexity. Traditional FBMC systems are difficult to implement. To effectively reduce the complexity of underwater acoustic FBMC systems, a fast implementation method is applied here [21]. The FBMC transmit signal $s(t)$ can be expressed as in Equations (6)–(8).

$$s(t) = s^R(t) + js^I(t - T/2) \tag{6}$$

$$s^R(t) = \sum_{n=0}^{N_s-1} \sum_{m=0}^{M-1} a_{n,m}^R e^{jm(2\pi t/T+\pi/2)} g(t-nT) \tag{7}$$

$$s^I(t) = \sum_{n=0}^{N_s-1} \sum_{m=0}^{M-1} a_{n,m}^I e^{jm(2\pi t/T+\pi/2)} g(t-nT) \tag{8}$$

where N_s denotes the number of FBMC symbols, M denotes the number of subcarriers, and T denotes the symbol interval. In Equations (7) and (8), $a_{n,m}^R$ and $a_{n,m}^I$ represent the real

and imaginary parts of the mapped complex sequence, respectively, and $g(t)$ denotes the prototype pulse filter.

The corresponding discrete signal equation is as follows:

$$s[i] \triangleq s(t)|_{t=iT_s} = s^R(iT_s) + js^I((i - M/2)T_s) \tag{9}$$

where $T_s \triangleq T/M$ is the sampling interval, $s^R(t)$ obtained through derivation is as follows:

$$\begin{aligned} s^R[i] \triangleq s^R(iT_s) &= \sum_{n=0}^{N_s-1} \sum_{m=0}^{M-1} a_{n,m}^R e^{jm((2\pi/T)iT_s+\pi/2)} g(iT_s - nMT_s) \\ &= \sum_{n=0}^{N_s-1} \sum_{m=0}^{M-1} a_{n,m}^R e^{jm((2\pi/M)i+\pi/2)} g((i - nM)T_s) \end{aligned} \tag{10}$$

where $d_n^{(R)}$ is a $M \times 1$ vector. The m-th component can be identified with $d_{n,m}^{(R)}$, which is equivalent to $s^R(nM + m)$; so, Equation (10) can be written as follows:

$$\begin{aligned} d_{n,m}^R \triangleq s^R[nM + m] &= \sum_{n'=0}^{N_s-1} \sum_{m'=0}^{M-1} a_{n',m'}^R e^{jm'[(2\pi/M)(nM+m)+(\pi/2)]} g((nM + m - n'M)T_s) \\ &= \sum_{n'=0}^{N_s-1} \sum_{m'=0}^{M-1} \left(j^{m'} a_{n',m'}^R\right) e^{jm'(2\pi/M)m} g((m + (n - n')M)T_s) \\ &= \sum_{n'=0}^{N_s-1} b_{n',m}^{(R)} g((m + (n - n')M)T_s) \end{aligned} \tag{11}$$

where $b_{n,m}^{(R)} = \sum_{m'=0}^{M-1} \left(j^{m'} a_{n,m'}^R\right) e^{jm'(2\pi/M)m}$, $b_{n,m}^{(R)}$ is the inverse discrete Fourier transform (IDFT) operation of $j^{m'} a_{n,m'}^R$, and $b_n^{(R)}$ is a $M \times 1$ vector. The m-th component can be identified with $b_{n,m}^{(R)}$, we get:

$$b_{n,m}^{(R)} = IDFT\left[\omega a_n^{(R)}\right] \tag{12}$$

where $\omega_m = j^{m'}$. Accordingly, Equation (12) can be further written as follows:

$$d_n^{(R)} = \sum_{n'=0}^{N_s-1} d_{n'}^{(R)} g_{n-n'} \tag{13}$$

The m-th component of g_n is as follows:

$$g_{n,m} \triangleq g((m + nM)T_s) \tag{14}$$

The prototype pulse $g(t)$ is non-zero only within range $[0, KT)$; therefore, g_n is non-zero within $n \in \{0, 1, \ldots, K-1\}$. Here, K is the overlap factor, and K = 4. Thus, Equation (13) can be expressed as follows:

$$d_n^{(R)} = \sum_{n'=0}^{N_s-1} d_{n'}^{(R)} g_{n-n'} \tag{15}$$

Based on the derivation process of $s^R(t)$, the expression of $s^I(t)$ can be directly obtained as follows:

$$d_n^{(I)} = g_0 b_n^{(I)} + g_1 b_{n-1}^{(I)} + \ldots + g_{K-1} b_{n-(K-1)}^{(I)} \tag{16}$$

where $b_{n,m}^{(I)} = IDFT\left[\omega a_n^I\right]$.

Based on the above derivation, the data generation structure of $s^R(t)$ can be obtained as shown in Figure 6.

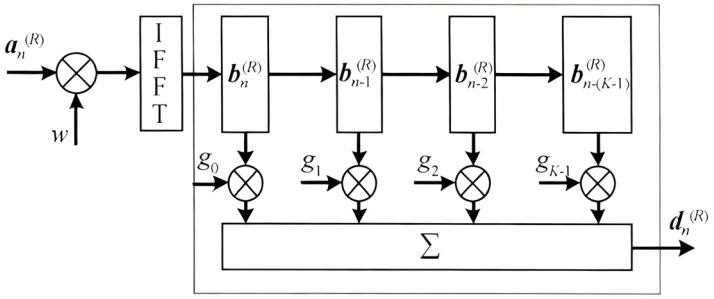


Figure 6. FBMC data generation structure diagram.

3. FBMC Channel Equalization Algorithm Based on Joint Time–Frequency Processing

Through optimized prototype pulse design and OQAM technology, FBMC/OQAM systems can ensure orthogonality in the real domain under ideal static channel conditions while minimizing the system's inherent inter-symbol interference (ISI) and inter-carrier interference (ICI). This provides a solid theoretical foundation for system performance [3,10]. However, this does not mean that equalization is unnecessary at the receiver. In practical applications, the underwater acoustic channel, featuring a long delay spread, strong multipath effects, and significant frequency-selective fading, will severely disrupt the orthogonality established by the prototype filter, introduce random and time-varying channel interference that is far stronger than the inherent interference, and cause severe distortion of the received signal (which becomes a complex signal containing residual interference and noise) [22]. Therefore, adopting complex domain equalization processing at the receiver can address channel distortion and effectively recover the signal. In this study, the MMSE and RLS equalizers operate in the complex domain, and the final output undergoes a real-part extraction operation before being used for OQAM demodulation.

To address this, this study proposes four time–frequency joint equalization schemes (ZF-RLS, ZF-LMS, MMSE-RLS, and MMSE-LMS). The joint equalization algorithms suppress the impact of frequency-selective fading through frequency-domain equalization algorithms while utilizing adaptive filtering in time-domain equalization to eliminate the influence of multipath delay. The synergistic effect of the two can significantly improve the transmission performance of the system in underwater acoustic channels. In this section, the formula derivation is carried out by taking the joint equalization algorithm of frequency-domain MMSE and time-domain RLS as an example, and the same logic applies to other time–frequency joint algorithms.

3.1. Frequency-Domain MMSE Pre-Equalization

Frequency-domain equalization (FDE) suppresses ICI by compensating for the frequency-selective fading of the channel [23,24]. It is assumed that the frequency-domain representation of the received signal after FFT is as follows:

$$Y(k) = H(k)X(k) + N(k) \tag{17}$$

where $H(k)$ is the channel frequency response, $X(k)$ is the transmitted signal, and $N(k)$ is additive noise. The coefficients of the MMSE-based frequency-domain equalizer are as follows:

$$W_{MMSE}(k) = \frac{H^*(k)}{|H(k)|^2 + \sigma_n^2} \tag{18}$$

where σ_n^2 is the noise power. The signal after frequency-domain equalization is as follows:

$$\hat{X}(k) = W_{MMSE}(k)Y(k) \tag{19}$$

Frequency-domain equalization can effectively compensate for the channel frequency response; however, in time-varying underwater acoustic channels, using frequency-domain equalization alone struggles to track the rapid changes of the channel. Therefore, it is necessary to combine it with time-domain equalization to further improve performance.

3.2. Time-Domain Equalization Algorithm

Time-domain equalization (TDE) suppresses ISI caused by multipath delays through adaptive filtering techniques [14,25]. This paper adopts the RLS algorithm to implement time-domain equalization, whose core idea is to update the filter coefficients by minimizing the weighted sum of squares of the error signals. Its objective function is as follows:

$$J(n) = \sum_{i=1}^{n} \lambda^{n-i} \left| d(i) - w^T(n)u(i) \right|^2 \tag{20}$$

where λ is the forgetting factor ($0 < \lambda \leq 1$), which controls the weight of historical data; $d(i)$ is the desired signal; $u(i)$ is the input signal vector; and $w(n)$ is the filter coefficient vector to be solved.

The iterative process of the RLS algorithm is as follows:

(1) Algorithm initialization: The filter coefficient vector is $w(0) = 0$, and the inverse correlation matrix is $P(0) = \delta^{-1}I$, where δ is a small positive number, usually ranging from 0.01 to 0.1, to avoid matrix singularity.

(2) Iterative update steps:

Step 1: calculate the a priori error:

$$e(n) = d(n) - w^T(n-1)u(n) \tag{21}$$

where $w(n-1)$ is the filter coefficient at the previous moment.

Step 2: calculate the gain vector:

$$k(n) = \frac{P(n-1)u(n)}{\lambda + u^T(n)P(n-1)u(n)} \tag{22}$$

The λ in the denominator is used to balance the weights of new and old data, with a typical value ranging from 0.95 to 0.995.

Step 3: update the filter coefficients:

$$w(n) = w(n-1) - k(n)e^*(n) \tag{23}$$

For complex signals, the conjugate of the error $e^*(n)$ needs to be taken; for real signals, $e(n)$ is used directly.

Step 4: update the inverse correlation matrix:

$$P(n) = \lambda^{-1}\left[P(n-1) - k(n)u^T(n)P(n-1)\right] \tag{24}$$

Recursive updating is implemented using the Sherman–Morrison formula to ensure computational efficiency.

The RLS algorithm features fast convergence, enabling it to effectively track the time-varying characteristics of underwater acoustic channels. However, its computational

complexity is relatively high. Therefore, it is necessary to combine it with frequency-domain equalization to achieve efficient equalization.

3.3. Time–Frequency Joint Equalization

Joint time–frequency-domain equalization (JTFDE) achieves efficient compensation for underwater acoustic channels by synergizing the advantages of frequency-domain and time-domain equalization.

3.3.1. Derivation of the JTFDE Model

The output of the received signal after frequency-domain MMSE pre-equalization is $\hat{X}(k)$ (Equation (19)), and the corresponding time-domain signal is obtained through IFFT:

$$\hat{x}(n) = IFFT\{\hat{X}(k)\} \tag{25}$$

Since frequency-domain equalization cannot completely eliminate time-varying multipath interference, the residual interference signal can be expressed as follows:

$$e_{res}(n) = x(n) - \hat{x}(n) \tag{26}$$

where $x(n)$ is the ideal interference-free time-domain signal. To suppress the residual interference, a time-domain RLS equalizer (Equation (23)) is introduced, whose input is $\hat{x}(n)$ and the output is as follows:

$$\widetilde{x}(n) = \sum_{l=0}^{L-1} w_l(n)\hat{x}(n-l) \tag{27}$$

where $w_l(n)$ is the l-th tap coefficient of the time-domain equalizer, and L is the length of the equalizer. The equalizer coefficients $w(n)$ are updated by minimizing the weighted sum of squares of the error signal $\varepsilon(n) = d(n) - \widetilde{x}(n)$ (Equation (20)).

To improve equalization performance, the signal after time-domain equalization is fed back to the frequency domain for secondary equalization. The specific steps are as follows:

1. Frequency-domain secondary equalization: perform FFT on 1 to obtain the frequency-domain signal 2, and recalculate the MMSE equalizer coefficients using the updated channel estimation.
$$W_{MMSE}^{(2)}(k) = \frac{\hat{H}^*(k)}{\left|\hat{H}(k)\right|^2 + \sigma_n^2} \tag{28}$$
where $\hat{H}(k)$ is the channel frequency response updated based on the signal after time-domain equalization
2. Iterative interference cancellation: Residual interference is gradually eliminated through multiple iterations. The frequency-domain equalization output of the i-th iteration is as follows:
$$\hat{X}^{(i)}(k) = W_{MMSE}^{(i)}(k)Y(k) \tag{29}$$
The output of the time-domain equalization is $\widetilde{x}^{(i)}(n)$ until the error converges ($\left\|\varepsilon^{(i)}(n)\right\| < \delta$).

3.3.2. Algorithm Flow

Figure 7 is a flowchart, and the specific process is as follows:

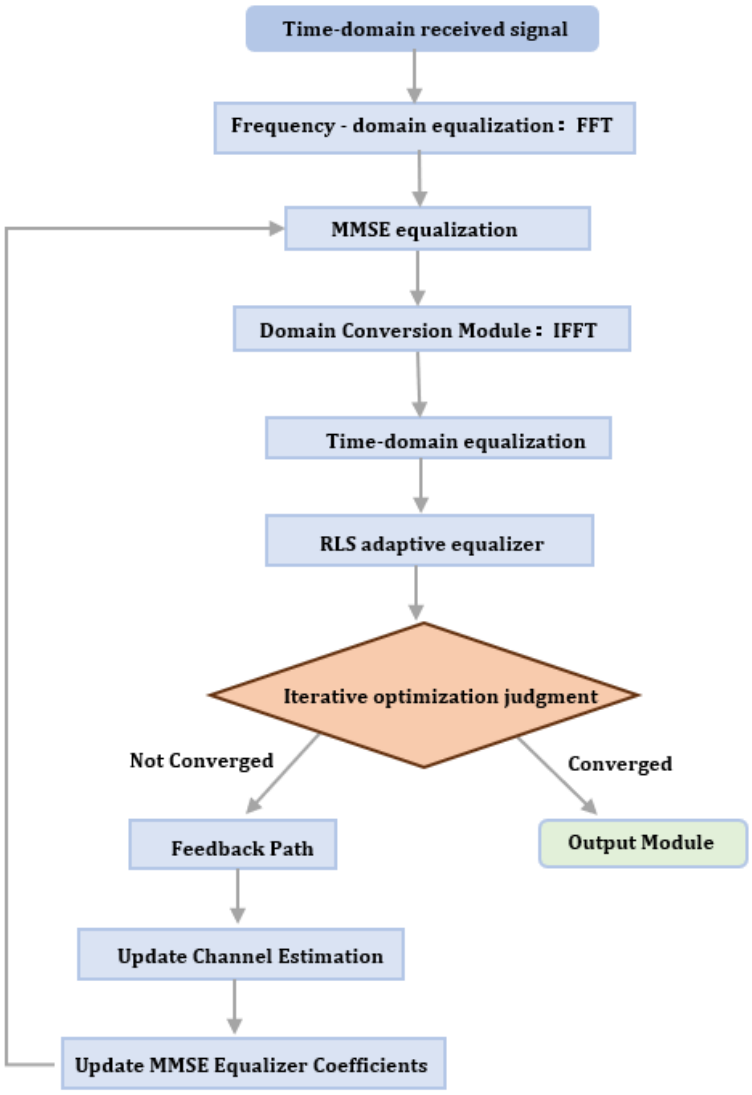


Figure 7. Algorithm flowchart.

Step 1: frequency-domain equalization: perform FFT on the received signal, use an MMSE equalizer to compensate for the channel frequency response, and obtain the initially equalized signal 1.

Step 2: time-domain equalization: first, perform IFFT on 1 to obtain the time-domain signal 2, and then use the RLS algorithm to further equalize 3 to eliminate residual multipath interference.

Step 3: iterative optimization: feed the time-domain equalized signal back to the frequency domain, recalculate the channel estimation, and update the equalizer coefficients until convergence is reached.

3.3.3. Complexity Analysis

The computational complexity of the time–frequency joint equalization algorithm mainly stems from two processing stages: the frequency domain and the time domain. The core operations of frequency-domain MMSE equalization lie in M-point FFT/IFFT operations and complex multiplication operations at each frequency bin. Its complexity is O(MlogM), which is comparable to the frequency-domain equalization complexity in traditional OFDM systems, thus granting it high computational efficiency. The introduction of the time-domain RLS adaptive equalizer is designed to track time-varying channels and eliminate residual interference, but this comes at the cost of higher computational

complexity. As the RLS algorithm requires iterative updates of the inverse correlation matrix, it has a computational complexity of $O(L^2)$ per symbol, where L denotes the number of equalizer taps. Compared with the O(L) complexity of algorithms such as LMS, this undoubtedly imposes higher requirements on the computational capability of the processor.

The joint architecture design proposed in this paper effectively alleviates the complexity burden of the RLS algorithm:

1. Preprocessing function of frequency-domain pre-equalization: The frequency-domain MMSE module first compensates for the main frequency-selective distortion of the channel through efficient FFT/IFFT operations, significantly reducing the degree of signal distortion. This enables a substantial reduction in the residual interference energy that the subsequent time-domain RLS equalizer needs to counteract; so, a shorter filter length L can be adopted. Since its complexity term is $O(L^2)$, a moderate reduction in L can significantly decrease the total computation load of the RLS component.
2. System-level benefits of convergence speed: The excellent convergence characteristics of the RLS algorithm enable it to require a much shorter training sequence than that of the LMS algorithm in rapidly time-varying channels. In terms of the average overhead for processing an entire data frame, the faster convergence speed of RLS can offset its higher single-point computational load-a feature that is particularly important in practical communication systems adopting frame structures.
3. Practical feasibility of parameter selection: Under the system parameters set in this study, the overall complexity of the algorithm is achievable for modern Digital Signal Processors (DSPs) or Field-Programmable Gate Arrays (FPGAs). In addition, this study also provides alternative combinations such as MMSE-LMS, offering flexibility for application scenarios with severely limited computing resources.

In summary, although the introduction of time-domain RLS equalization brings relatively high computational complexity, the proposed joint equalization scheme achieves a good balance between computational complexity and system performance through the effective burden-sharing of frequency-domain preprocessing and the improvement in overall system efficiency, and thus has the potential to be applied in practical underwater acoustic communication systems.

4. Simulation and Discussion Analysis

To verify the performance advantages of the time–frequency joint equalization algorithm proposed in this study in the underwater acoustic FBMC/OQAM system, simulation experiments of the system are designed as follows: (1) Compare and analyze the bit error rate (BER) and constellation diagram characteristics of frequency-domain equalization (FDE), time-domain equalization (TDE), and JTFDE to verify the effectiveness of the proposed algorithm in suppressing multipath interference and tracking time-varying channels. (2) Investigate the adaptability of the algorithm to different modulation orders through performance comparison between 4QAM and 16QAM modulation schemes. (3) Finally, conduct an optimization analysis on the key parameters (forgetting factor λ and step size factor μ) of the time-domain equalizer to provide a theoretical basis for parameter configuration in practical systems.

4.1. Simulation Conditions and Parameter Settings

To ensure the authenticity and reliability of the experimental results, the underwater acoustic channel data used in this study were obtained from the Qingjiang Section in Yichang, Hubei Province, as shown in Table 3. The parameter settings for the simulation experiments are listed in Table 3.

Table 3. Simulation parameter.

Simulation Parameter	Simulation Values
Sampling Rate	128 kHz
Number of Subcarriers	256
Baseband Bandwidth	6.4 KHz
Frequency Range	12.8 kHz–19.2 kHz
Subcarrier Spacing	25 Hz
Constellation Mapping	4QAM
Filter	PHYDYAS (K = 4)

Figure 8 illustrates the simulation of the underwater acoustic multipath channel using the Monte Carlo method, and the impulse response of the channel is shown in Figure 9. It can be observed that the underwater acoustic channel environment is relatively complex, with severe multipath effects, leading to significant intersymbol interference between signals.

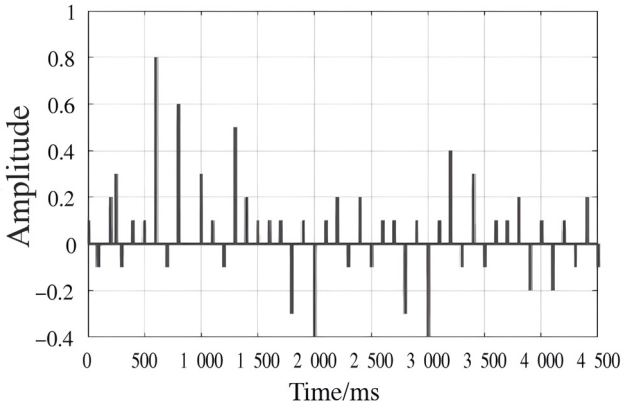


Figure 8. Simulated underwater acoustic multipath channel.

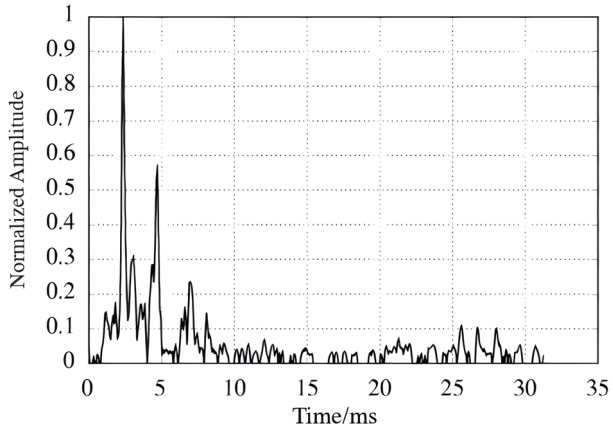


Figure 9. Impulse response diagram of underwater acoustic channel at a certain moment.

4.2. Performance Analysis of Time–Frequency Joint Equalization Algorithm

4.2.1. Algorithm Performance Comparison

This section evaluates the core performance metrics of the joint time–frequency equalization algorithm [26]. First, based on the bit error rate (BER) and constellation diagram characteristics, the proposed JTFDE is compared with FDE and TDE. The focus is on comparing the performance differences between the four joint time–frequency equalization

schemes, ZF-RLS, ZF-LMS, MMSE-RLS, and MMSE-LMS, in terms of multipath interference suppression and time-varying channel tracking.

Figure 10 compares the performance of ZF, RLS, LMS, MMSE, and the time–frequency joint equalization algorithms ZF-RLS, ZF-LMS, MMSE-RLS, and MMSE-LMS in terms of BER in the FBMC/OQAM system. The experimental results show that the four combined equalization algorithms exhibit superior performance in terms of BER. Additionally, the MMSE-based algorithms MMSE-RLS and MMSE-LMS outperform the ZF-based algorithms ZF-RLS and ZF-LMS overall owing to the MMSE-based algorithms' ability to suppress interference while also mitigating noise. Among the MMSE-RLS and MMSE-LMS algorithms, the RLS algorithm outperforms the LMS algorithm due to its stronger adaptive capabilities. Based on the simulation results, MMSE-RLS performs best at medium-to-high signal-to-noise ratios, owing to the synergistic effect of frequency-domain MMSE pre-equalization and time-domain RLS adaptive filtering, which effectively suppresses multipath interference and time-varying channel effects. At low signal-to-noise ratios, the performance of all algorithms is similar. Time–frequency joint equalization algorithms, such as MMSE-RLS, enhance the system's interference resistance through fast compensation in the frequency domain and dynamic tracking in the time domain, thereby validating the superiority of joint processing. Therefore, joint time–frequency equalization algorithms are more suitable for complex underwater acoustic channel environments than other methods.

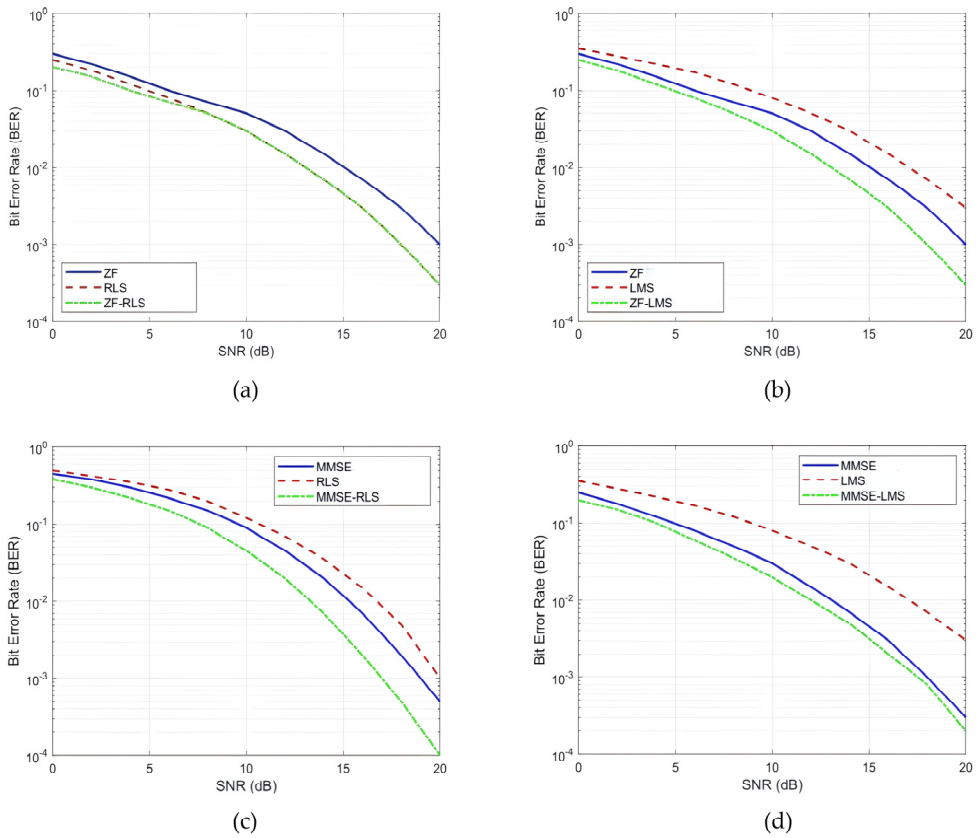


Figure 10. BER performance of the system under different equalization algorithms. (**a**) BER performance of ZF, RLS, and ZF-RLS joint equalization algorithms; (**b**) BER performance of ZF, LMS, and ZF-LMS joint equalization algorithms; (**c**) BER performance of MMSE, RLS, and MMSE-RLS joint equalization algorithms; (**d**) BER performance of MMSE, LMS, and MMSE-LMS joint equalization algorithms.

Figure 11 shows the comparison results of constellation diagrams of received signals processed by six different equalization algorithms (ZF, MMSE, ZF-RLS, ZF-LMS, MMSE-RLS, and MMSE-LMS) in the FBMC/OQAM system when the signal-to-noise ratio

(SNR) is 20 dB. Observing the results, it can be seen that although frequency-domain equalization algorithms ZF and MMSE can initially compensate for channel distortion, there is still an obvious diffusion phenomenon in the constellation points, indicating that residual interference has not been completely eliminated. In contrast, the constellation diagrams of time–frequency joint equalization algorithms (ZF-RLS, ZF-LMS, MMSE-RLS, and MMSE-LMS) show clearer clustering effects; especially of note, the constellation points of the MMSE-RLS algorithm are the most concentrated and compact. This verifies that time-domain adaptive equalization can effectively suppress the residual inter-symbol interference after frequency-domain equalization. In addition, MMSE-based algorithms have better convergence of constellation points than ZF-based algorithms, which is consistent with the BER performance trend in Figure 7. This further illustrates the comprehensive advantages of the MMSE-RLS combination in interference suppression and noise robustness in time–frequency joint processing. These results intuitively reflect that time–frequency joint equalization improves the quality of signal recovery through collaborative processing.

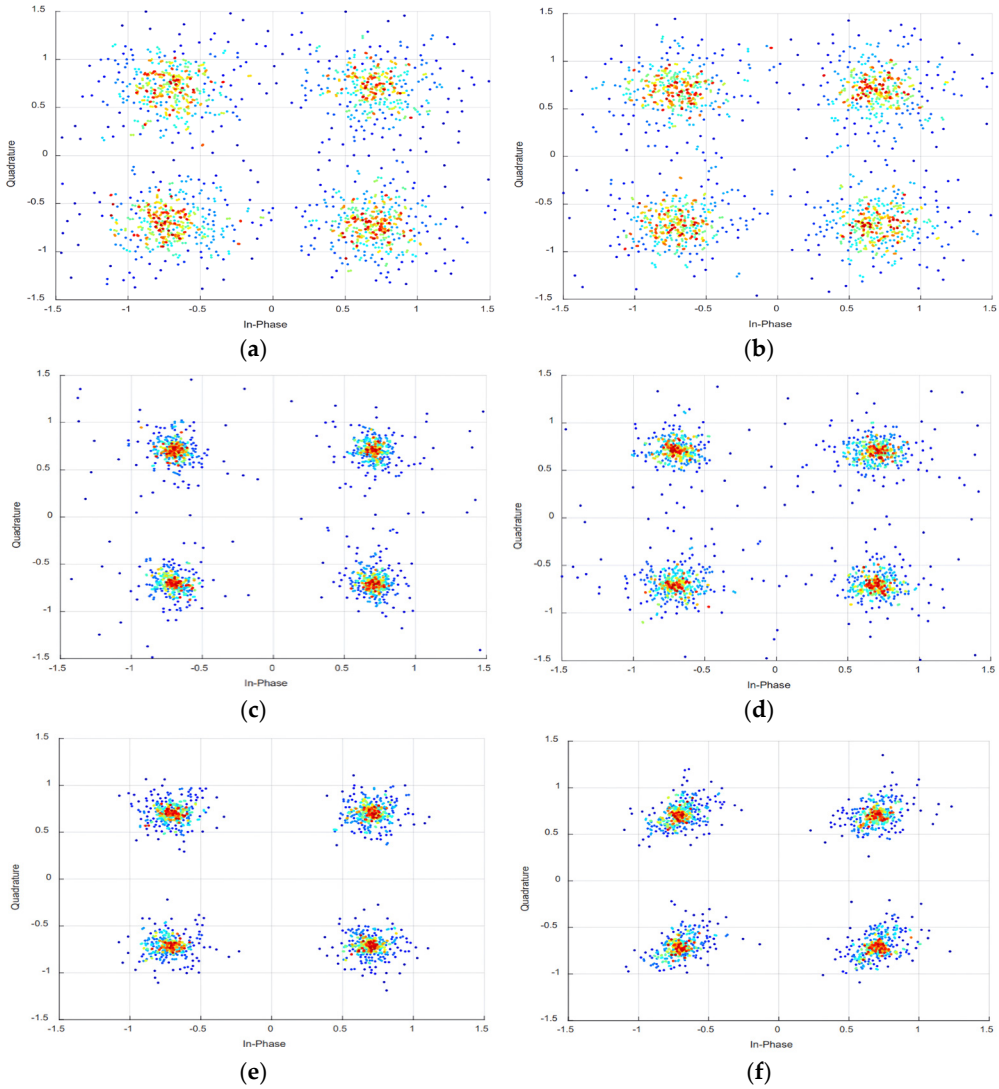


Figure 11. Constellation diagrams of received data after equalization at SNR = 20 dB. (**a**) ZF equalization; (**b**) MMSE equalization; (**c**) ZF-RLS equalization; (**d**) ZF-LMS equalization; (**e**) MMSE-RLS equalization.; (**f**) MMSE-LMS equalization.

Figure 12 shows the performance comparison curves of BER versus SNR for different equalization algorithms in underwater acoustic channels. From the overall trend, the

BER of all algorithms decreases with the increase in SNR, but there are significant differences in the decline rate. The time–frequency joint equalization algorithms, especially the MMSE-RLS combination, always maintain an optimal performance, with their BER curves located at the bottom. In comparison, the performance of the single frequency-domain equalization algorithm MMSE is slightly inferior, while the ZF-based algorithms show the worst performance. It is worth noting that in the medium- and high-SNR regions, the time–frequency joint equalization exhibits more significant performance advantages over the single frequency-domain equalization, which verifies the suppression effect of time-domain adaptive equalization on residual interference. These results fully indicate that in complex underwater acoustic channel environments, time–frequency joint equalization can more effectively overcome multipath effects and time-varying interference through the collaborative processing in frequency and time domains, thereby achieving better system performance.

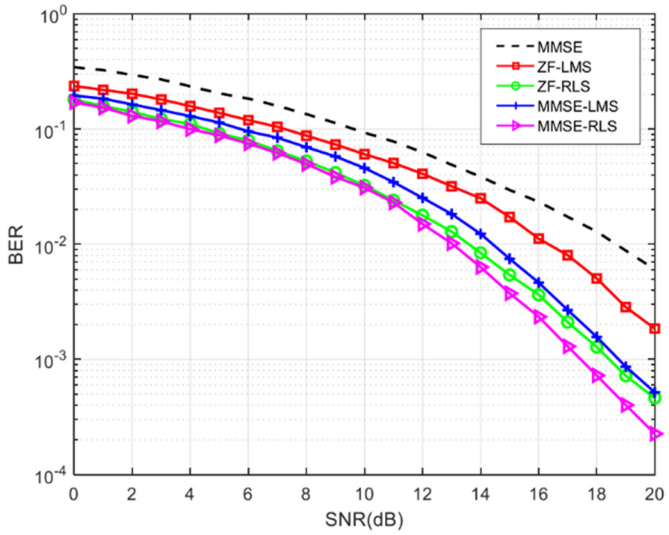


Figure 12. BER performance curves of equalization algorithms.

To comprehensively evaluate the performance of the proposed algorithm, this paper compares the MMSE-RLS algorithm with two advanced schemes: Sparse Bayesian Learning (SBL) and Turbo equalization. As can be observed from Figure 13 of the simulation results, the MMSE-RLS scheme proposed in this study achieves the optimal performance, with its BER significantly lower than that of the comparison algorithms across the entire SNR range. The Turbo equalization scheme ranks second in performance, yet its BER curve consistently lies above that of MMSE-RLS. In contrast, the equalizer based on SBL exhibits poor performance, which is far inferior to that of the other two schemes. Particularly when the SNR exceeds 10 dB, the performance gap widens sharply. This indicates that under the underwater acoustic FBMC/OQAM system and channel environment configured in this study, the sparse prior assumption relied on by the SBL algorithm may be invalid, or its iterative process may fail to converge—preventing its theoretical advantages from being realized.

While it achieves performance superiority, the MMSE-RLS scheme in this paper also features low implementation complexity. The SBL scheme, which performs the worst, involves high-dimensional matrix inversion and complex iterations, resulting in the greatest difficulty in engineering implementation. The Turbo equalization scheme, with intermediate performance, relies on iterative soft information processing and decoding procedures, leading to high computational complexity and processing delay. In comparison, the core operations of the MMSE-RLS scheme are only FFT/IFFT (which is efficient and easy for

hardware implementation) and RLS adaptive filtering. It has a clear structure and low resource consumption, providing a balanced solution for the engineering deployment of FBMC/OQAM systems.

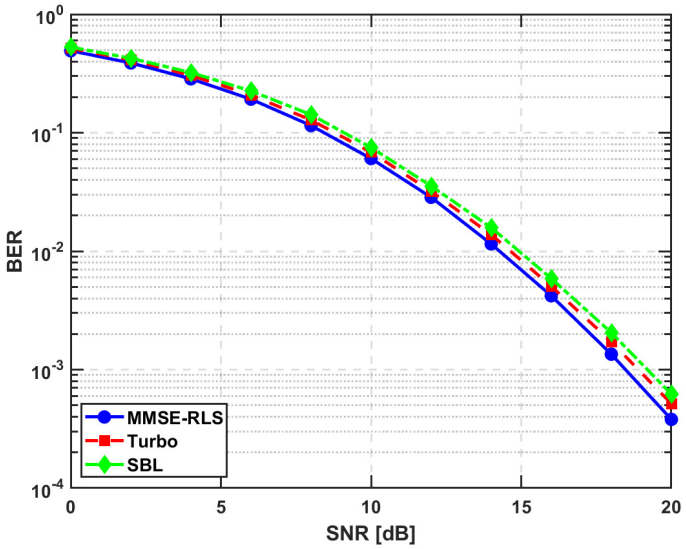


Figure 13. Comparison experiments between MMSE-RLS, SBL, and turbo equalization.

4.2.2. The Impact of Modulation Schemes on Performance

To analyze the impact of modulation orders on equalization algorithms, this study compares the system performance under 4QAM and 16QAM modulations with the experimental results shown in Figure 14. As can be seen from the results, the BER performance of 4QAM is significantly better than that of 16QAM, mainly because higher-order modulation is more sensitive to channel distortion and noise. Although different equalization algorithms maintain a consistent performance ranking under the two modulation schemes—MMSE outperforms ZF, and RLS is superior to LMS—with the increase in SNR, the BER of 16QAM decreases at a significantly slower rate than that of 4QAM, and the performance gap between the two gradually widens. This indicates that low-order modulation schemes such as 4QAM should be preferred when channel conditions are poor. In scenarios with good channel conditions where spectral efficiency is pursued, 16QAM can be considered, but it needs to be paired with more powerful equalization algorithms to ensure system performance.

4.2.3. Parameter Optimization Analysis

The parameter settings of the time-domain equalizer have a significant impact on algorithm performance. Therefore, this section compares the performance of 4QAM under the forgetting factor λ of the RLS algorithm and the step size factor μ of the LMS algorithm. The simulation results, as shown in Figures 15 and 16, present the BER performance of the LMS and RLS algorithms under different parameter configurations.

Figure 15 shows the comparison of BER performance of the FBMC system with the 4QAM modulation scheme under different λ values. The results indicate that for the RLS algorithm, a smaller λ (e.g., λ = 0.95) assigns higher weights to new data, which improves the convergence speed of the algorithm but makes it more sensitive to noise. A larger λ (e.g., 0.99) enhances the influence of historical data, suppresses noise, but reduces the dynamic tracking capability. λ = 0.98 achieves the optimal balance between convergence speed and steady-state error, thereby minimizing the overall mean square error (MSE) of the MMSE-RLS algorithm.

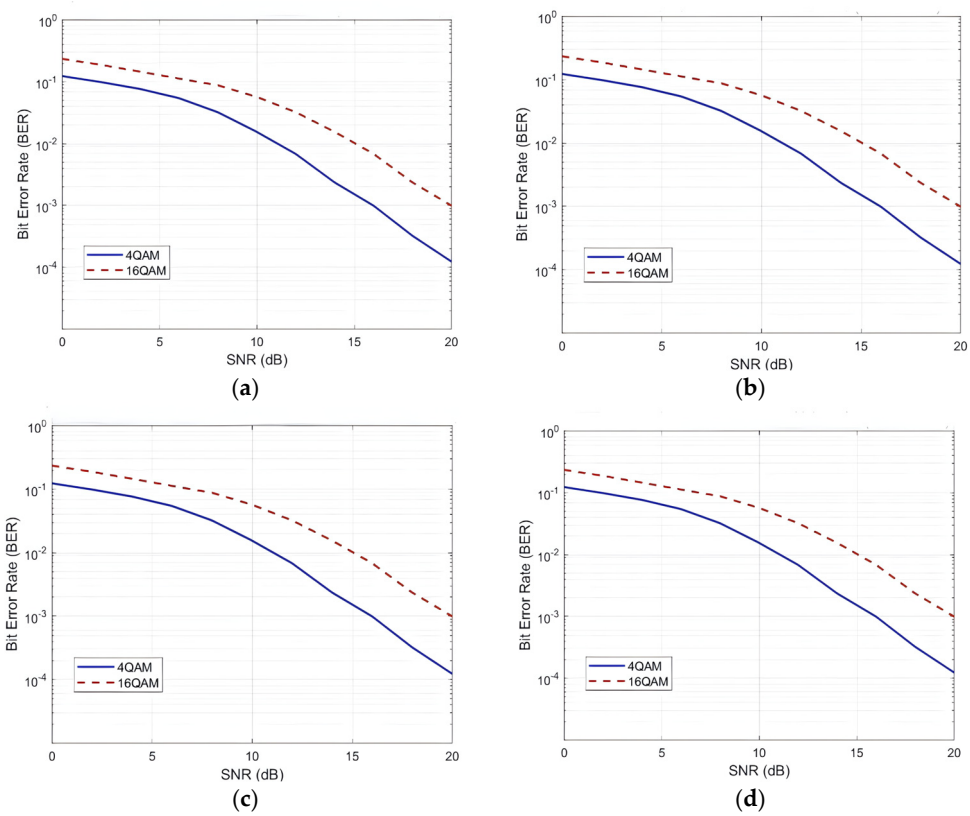


Figure 14. BER performance of the system under different baseband modulations. (**a**) ZF-RLS equalization, λ = 0.99; (**b**) ZF-LMS equalization, μ = 0.005; (**c**) MMSE-RLS equalization, λ = 0.99; (**d**) MMSE-LMS equalization, μ = 0.005.

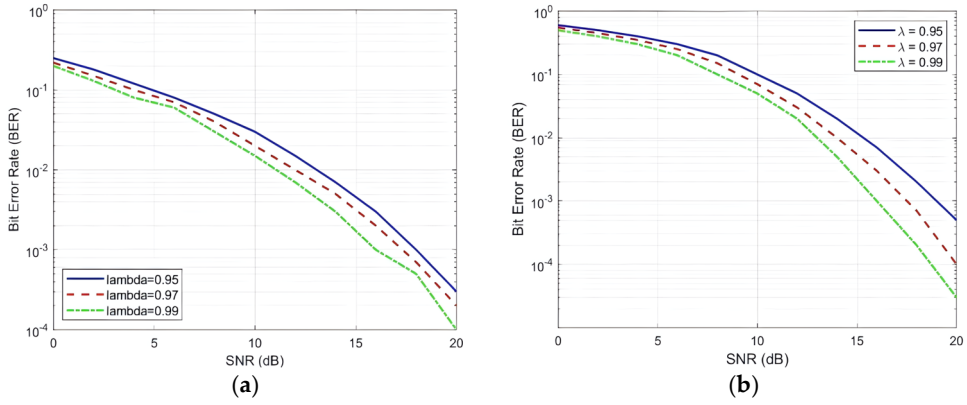


Figure 15. BER performance of the FBMC system with 4QAM modulation scheme under different λ values. (**a**) ZF-RLS; (**b**) MMSE-RLS.

Figure 16 shows the comparison of BER performance of the FBMC system with the 4QAM modulation scheme under different μ values. The results indicate that for the LMS algorithm, the selection of the step size factor μ is crucial. A smaller μ value, such as 0.01, can improve steady-state accuracy but results in slower convergence, while a larger μ value, such as 0.1, accelerates convergence but may sacrifice stability. MMSE-LMS achieves the optimal balance when μ = 0.05. Overall, parameter optimization requires a trade-off between convergence speed and steady-state error. MMSE-based algorithms exhibit stronger robustness to parameter variations, which verifies the necessity of adaptive parameter adjustment in time–frequency joint equalization.

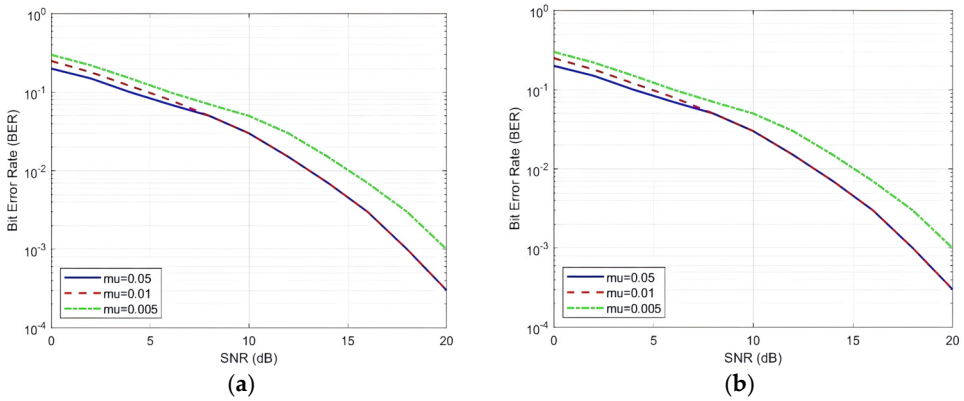


Figure 16. BER performance of the FBMC system with 4QAM modulation scheme under different μ Values. (**a**) ZF-LMS; (**b**) MMSE-LMS.

4.2.4. Time-Varying Channel Tracking Performance

To quantitatively evaluate the tracking capability of the proposed algorithm under time-varying channels, Figure 17 plots the normalized mean square error (NMSE) performance curves of the MMSE-RLS, ZF-RLS, and pure time-domain RLS algorithms under the condition of SNR ranging from 0 to 20 dB with a step size of 2 dB. It can be observed that the joint scheme based on MMSE pre-equalization (MMSE-RLS) exhibits the optimal NMSE performance across the entire SNR range. This confirms that frequency-domain MMSE preprocessing effectively suppresses initial distortion and noise, providing the time-domain RLS equalizer with better input signal conditions. The two work synergistically, significantly enhancing the overall tracking capability and equalization accuracy for time-varying channels.

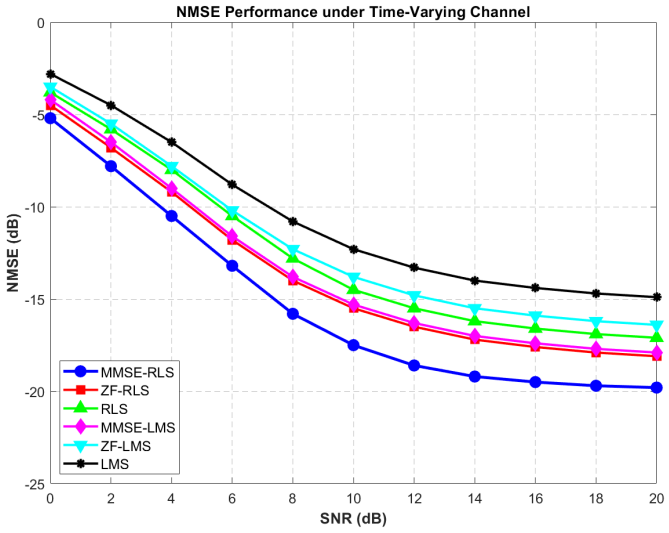


Figure 17. Comparison of NMSE performance among different equalization algorithms under underwater acoustic time-varying channels.

5. Conclusions

This paper investigated channel equalization techniques in underwater acoustic FBMC/OQAM systems. Aiming at the time-varying characteristics of underwater acoustic channels and the inherent interference of the system, a time–frequency joint equalization algorithm was proposed. The algorithm initially eliminated multipath interference through frequency-domain MMSE equalization, combined time-domain RLS adaptive decision feedback equalization to dynamically track channel changes, and adopted iterative inter-

ference cancellation technology to gradually eliminate residual imaginary interference. The simulation results showed that compared with single frequency-domain equalization and time-domain adaptive equalization, the proposed time–frequency joint equalization scheme significantly improved the bit error rate performance, among which the MMSE-RLS combination exhibited the optimal equalization effect under medium and high signal-to-noise ratio conditions. Through performance comparison under different modulation schemes (4QAM and 16QAM), the adaptability of the algorithm in various transmission environments was verified. This research also indicated that reasonably setting the step size factor and forgetting factor parameters of the time-domain equalizer could further optimize the system performance. This finding provided an effective equalization solution for underwater acoustic FBMC systems to cope with the challenges of time-varying multipath channels.

Author Contributions: Methodology, W.H.; Formal analysis, M.Z.; Data curation, L.Y.; Writing–original draft, Y.W. All authors have read and agreed to the published version of the manuscript.

Funding: This research was funded by the National Key Laboratory of Wireless Communications Foundation, grant number IFN20230113; National Natural Science Foundation of China, grant number 62105093.

Data Availability Statement: The original contributions presented in this study are included in the article. Further inquiries can be directed to the corresponding author.

Conflicts of Interest: The authors declare no conflict of interest.

References

1. Ma, Y.; Zhang, Q.; Wang, H. 6G: Ubiquitously extending to the vast underwater world of the oceans. *Engineering* **2022**, *8*, 12–17. [CrossRef]
2. Hilal, A.S. and Al-Kindi, M.J. Design of filter bank for multicarrier (FBMC). *Int. J. Sci. Eng. Res.* **2020**, *11*, 608–616.
3. Song, Z. Performance evaluation of prototype filter-based FBMC/OQAM system for wireless communications. In *Proceedings of the 2024 4th Asia-Pacific Conference on Communications Technology and Computer Science (ACCTCS), Shenyang, China, 24–26 February 2024*; IEEE: New York, NY, USA, 2024; pp. 776–779.
4. Kadhem, O.F.; Jamel, T.M.; Khazaal, H.F. An Overview for Channel Equalization Techniques in Filter Bank. In *Proceedings of the 2023 Second International Conference on Advanced Computer Applications (ACA), Maysan, Iraq, 27–28 February 2023*; IEEE: New York, NY, USA, 2023; pp. 7–12.
5. Saideh, M.; Dayoub, I.; Berbineau, M. Efficient equalization for FBMC-OQAM under doubly selective channel estimation errors. *IEEE Commun. Lett.* **2019**, *23*, 863–866. [CrossRef]
6. Wang, Y.; Guo, Q.; Xiang, J.; Liu, Y. Doubly selective channel estimation and equalization based on ICI/ISI mitigation for OQAM-FBMC systems. *Phys. Commun.* **2023**, *59*, 102120. [CrossRef]
7. Jing, L.; Zheng, T.; He, C.; Yin, H. Iterative adaptive frequency-domain equalization based on sliding window strategy over time-varying underwater acoustic channels. *JASA Express Lett.* **2021**, *1*, 076002. [CrossRef] [PubMed]
8. Feng, C.; Luo, Y.; Zhang, J.; Li, H. An OFDM-based frequency domain equalization algorithm for underwater acoustic communication with a high channel utilization rate. *J. Mar. Sci. Eng.* **2023**, *11*, 415. [CrossRef]
9. Lu, X.; Jiang, Y.; Wei, Y.; Tu, X.; Qu, F. A Lattice-reduction-aided sphere decoder for underwater acoustic FBMC/OQAM communications. *IEEE Wirel. Commun. Lett.* **2022**, *12*, 466–470. [CrossRef]
10. Elghetany, S.E.; Hassaneen, S.; Shaalan, I.E.; Soliman, H.Y. Channel estimation techniques based on intrinsic interference mitigation for FBMC/OQAM systems. *Comput. Electr. Eng.* **2024**, *117*, 109244. [CrossRef]
11. Lai, K.C.; Huang, Y.J.; Chen, C.T.; Lin, C.F. A family of MMSE-based decision feedback equalizers and their properties for FBMC/OQAM systems. *IEEE Trans. Veh. Technol.* **2019**, *68*, 2346–2360. [CrossRef]
12. Lakew, W.; Al-Dweik, A.; Assaf, T. Performance Analysis of OFDM-SIMO Systems with Time-Domain Interleaving. *IEEE Commun. Lett.* **2024**, *29*, 323–327. [CrossRef]
13. Zegrar, S.E.; Arslan, H. Common CP-OFDM transceiver design for low-complexity frequency domain equalization. *IEEE Wirel. Commun. Lett.* **2022**, *11*, 1349–1353. [CrossRef]
14. Tu, X.; Wei, Y.; Qu, F.; Song, A. Low computational complexity RLS-based decision-feedback equalization in underwater acoustic communications. *IEEE J. Ocean. Eng.* **2024**, *49*, 1067–1088. [CrossRef]

15. Zheng, T.; Jing, L.; Long, C.; He, C.; Yin, H. Frequency domain direct adaptive turbo equalization based on block normalized minimum-SER for underwater acoustic communications. *Appl. Acoust.* **2023**, *205*, 109266. [CrossRef]
16. Kadhem, O.F.; Jamel, T.M.; Khazaal, H.F. Equalization methods for Filter Bank Multicarrier OQAM. *Wasit J. Eng. Sci.* **2023**, *11*, 106–119. [CrossRef]
17. Ruigang, H.; Ning, J.; Biao, L.; Jianchun, H.; Shengming, G. A Study of Time Domain Adaptive Decision Feedback MSK Equalization over Time-varying Underwater Acoustic Channel. In *Proceedings of the 2021 OES China Ocean Acoustics (COA), Harbin, China, 14–17 July 2021*; IEEE: New York, NY, USA, 2021; pp. 591–595.
18. Han, R.; Jia, N.; Huang, J.; Guo, S. Joint time-frequency domain equalization of MSK signal over underwater acoustic channel. *Appl. Acoust.* **2022**, *189*, 108597. [CrossRef]
19. Wang, H.; Li, X.; Jhaveri, R.H.; Gadekallu, T.R.; Zhu, M.; Ahanger, T.A.; Khowaja, S.A. Sparse Bayesian learning based channel estimation in FBMC/OQAM industrial IoT networks. *Comput. Commun.* **2021**, *176*, 40–45. [CrossRef]
20. Al-Dulaimi, M.A.; Cseppentő, B.; Kollár, Z. Comparison of Prototype Filters for FBMC-OQAM Systems. In *Proceedings of the 2025 35th International Conference Radioelektronika (RADIOELEKTRONIKA), Hnanice, Czechia, 12–14 May 2025*; IEEE: New York, NY, USA, 2025; pp. 1–5.
21. Mattera, D.; Tanda, M.; Bellanger, M. Performance analysis of some timing offset equalizers for FBMC/OQAM systems. *Signal Process.* **2015**, *108*, 167–182. [CrossRef]
22. Fhima, H.; Chang, B.S.; Zayani, R.; Shaiek, H.; Roviras, D.; Bouallegue, R. Performance of linear and widely linear equalizers for FBMC/OQAM modulation. In *Proceedings of the 2018 25th international conference on telecommunications (ICT), Saint-Malo, France, 26–28 June 2018*; IEEE: New York, NY, USA, 2018.
23. Marijanovic, L.; Schwarz, S.; Rupp, M. MMSE equalization for FBMC transmission over doubly-selective channels. In *Proceedings of the 2016 International Symposium on Wireless Communication Systems (ISWCS), Poznan, Poland, 20–23 September 2016*; IEEE: New York, NY, USA, 2016.
24. Chen, C.-W.; Maehara, F. An enhanced MMSE subchannel decision feedback equalizer with ICI suppression for FBMC/OQAM systems. In *Proceedings of the 2017 International Conference on Computing, Networking and Communications (ICNC), Silicon, VA, USA, 26–29 January 2017*; IEEE: New York, NY, USA, 2017.
25. Hamdan, A.; Hijazi, H.; Ros, L.; Al-Ghouwayel, A.; Siclet, C. Equalization with Time Domain Preprocessing for OFDM and FBMC in Flat Fading Fast Varying Channels. In *Proceedings of the 2022 IEEE 6th International Symposium on Telecommunication Technologies (ISTT), Johor Bahru, Malaysia, 14–16 November 2022*; IEEE: New York, NY, USA, 2022; pp. 91–96.
26. Indiarto, M.; Siswono, H. Analysis of Equalizer Performance against Bit Error Rate in Filter Bank Multicarrier System with AWGN and Multipath Channel. *Int. J. Comput. Appl.* **2021**, *183*, 21–25. [CrossRef]

Disclaimer/Publisher's Note: The statements, opinions and data contained in all publications are solely those of the individual author(s) and contributor(s) and not of MDPI and/or the editor(s). MDPI and/or the editor(s) disclaim responsibility for any injury to people or property resulting from any ideas, methods, instructions or products referred to in the content.